

Neural Network-based Reconstruction in Compressed Sensing MRI Without Fully-sampled Training Data

Alan Q. Wang¹, Adrian V. Dalca^{2,3}, and Mert R. Sabuncu^{1,4}

¹ School of Electrical and Computer Engineering, Cornell University

² Computer Science and Artificial Intelligence Lab at the Massachusetts Institute of Technology

³ A.A. Martinos Center for Biomedical Imaging at the Massachusetts General Hospital

⁴ Meinig School of Biomedical Engineering, Cornell University.

Abstract. Compressed Sensing MRI (CS-MRI) has shown promise in reconstructing under-sampled MR images, offering the potential to reduce scan times. Classical techniques minimize a regularized least-squares cost function using an expensive iterative optimization procedure. Recently, deep learning models have been developed that model the iterative nature of classical techniques by unrolling iterations in a neural network. While exhibiting superior performance, these methods require large quantities of ground-truth images and have shown to be non-robust to unseen data. In this paper, we explore a novel strategy to train an unrolled reconstruction network in an unsupervised fashion by adopting a loss function widely-used in classical optimization schemes. We demonstrate that this strategy achieves lower loss and is computationally cheap compared to classical optimization solvers while also exhibiting superior robustness compared to supervised models. Code is available at <https://github.com/alanqrwang/HQSNet>.

Keywords: Compressed sensing MRI · Unsupervised reconstruction · Model robustness

1 Introduction

Magnetic resonance (MR) imaging can be accelerated via under-sampling k -space – a technique known as Compressed Sensing MRI (CS-MRI) [25]. This yields a well-studied ill-posed inverse problem. Classically, this problem is reduced to regularized regression, which is solved via an iterative optimization scheme, e.g., [5,7,8,11,14,38], on each collected measurement set. The limitations of this instance-based optimization approach are well-known; solutions are heavily influenced by the choice of regularization function and can lack in high-frequency detail. Furthermore, they are often time-consuming to compute.

There has been a recent surge in deep learning methods for CS-MRI, which promise superior performance and computational efficiency. To date, these meth-

ods have largely relied on fully-sampled data, which are under-sampled retrospectively to train the neural network model. The primary focus of this body of research has been the design of the neural network architecture. So-called “unrolled architectures” [1,20,24,26,32,34,37] which inject the MR-specific forward model into the network architecture have been shown to outperform more general-purpose, black-box [23,24,35] models and aforementioned classical methods.

While these methods exhibit state-of-the-art reconstruction performance, a major limitation of the supervised formulation is the necessity for a dataset of fully-sampled ground-truth images, which can be hard to obtain in the clinical setting. In addition, these models are known to exhibit poor robustness at test-time when subjected to noisy perturbations and adversarial attacks [2].

In this work, we present a novel approach for performing MR reconstruction that combines the robustness of classical techniques with the performance of unrolled architectures. Specifically, we implement an unrolled neural network architecture that is trained to minimize a classical loss function, which does not rely on fully-sampled data. This is an “amortized optimization” of the classical loss, and we refer to our model as “unsupervised”. We show that our unsupervised model can be more robust than its supervised counterpart under noisy scenarios. Additionally, we demonstrate that not only can we replace an expensive iterative optimization procedure with a simple forward pass of a neural network, but also that this method can outperform classical methods even when trained to minimize the same loss.

2 Background

In the CS-MRI formulation, fully-sampled MR images are assumed to be transformed into under-sampled k -space measurements by the forward model:

$$y = \mathcal{F}_\Omega x, \quad (1)$$

where $x \in \mathbb{C}^N$ is the unobserved fully-sampled image, $y \in \mathbb{C}^M$ is the under-sampled k -space measurement vector⁵, $M < N$, and \mathcal{F}_Ω denotes the under-sampled Fourier operator with Ω indicating the index set over which the k -space measurements are sampled. For each instance y , classical methods solve the ill-posed inverse problem via an optimization of the form:

$$\arg \min_x \|\mathcal{F}_\Omega x - y\|_2^2 + \mathcal{R}(x), \quad (2)$$

where $\mathcal{R}(x)$ denotes a regularization loss term. The regularization term is often carefully engineered to restrict the solutions to the space of desirable images. Common choices include sparsity-inducing norms of wavelet coefficients [16], total variation [21,31], and their combinations [25,30]. The first term of Eq. (2),

⁵ In this paper, we assume a single coil acquisition.

called the data consistency term, quantifies the agreement between the measurement vector y and reconstruction x .

Half-quadratic splitting (HQS) [18,28] solves Eq. (2) by decoupling the minimization of the two competing terms using an auxiliary variable z and an alternating minimization strategy over iterations $k \in \mathbb{N}$:

$$z_k = \arg \min_z \mathcal{R}(z) + \lambda \|z - x_k\|_2^2, \quad (3a)$$

$$x_{k+1} = \arg \min_x \|\mathcal{F}_\Omega x - y\|_2^2 + \lambda \|z_k - x\|_2^2, \quad (3b)$$

where $\lambda \geq 0$ is a hyper-parameter. Eq. (3b) has closed-form solution in k -space at the sampling location m given by:

$$\hat{x}_{k+1}[m] = \begin{cases} \frac{y[m] + \lambda \hat{z}_k[m]}{1 + \lambda}, & \text{if } m \in \Omega \\ \hat{z}_k[m], & \text{else} \end{cases} \quad (4)$$

for all k , where \hat{x}_{k+1} and \hat{z}_k denote x_{k+1} and z_k in Fourier domain, respectively. The z -minimization of Eq. (3a) is the proximal operator for the regularizer, which may be solved using (sub-)gradient descent for differentiable \mathcal{R} . In this paper, we view the proximal operator as a function, i.e. $z_k = g(x_{k+1})$, where g is some neural network. HQS and its data-driven variants underlie algorithms in CS-MRI [1,32], image super-resolution [10], and image restoration [15].

Supervised deep learning offers an alternative approach. Given a dataset of fully-sampled images and (often retrospectively-created) under-sampled measurements $\mathcal{D} = \{(x_i, y_i)\}_{i=1}^N$, these methods learn the optimal parameters θ of a parameterized mapping $G_\theta : y_i \rightarrow x_i$ by minimizing:

$$\arg \min_\theta \frac{1}{N} \sum_{i=1}^N \mathcal{L}_{sup}(G_\theta(y_i), x_i), \quad (5)$$

where \mathcal{L}_{sup} is a loss function that quantifies the quality of reconstructions based on the fully-sampled x . This formulation obviates the need for the design of a regularization loss function. The parameterized mapping is often a neural network model [3,23,24,35]. Recently, unrolled architectures that exploit knowledge of the forward model [1,26,32] have proven to be effective. These architectures implement layers that iteratively minimize the data consistency loss and remove aliasing artifacts by learning from fully-sampled data. $K \in \mathbb{N}$ such blocks are concatenated and trained end-to-end to minimize the supervised loss of Eq. (5).

3 Proposed Method

To remove the need for fully-sampled data, leverage the robustness of the classical optimization method, and incorporate the performance of deep learning models, we propose to use an unsupervised strategy with an unrolled reconstruction architecture, which we call HQS-Net. Let a parameterized mapping G_θ denote a

neural network that maps under-sampled measurements to reconstructed images. We train this network to minimize over θ :

$$\mathcal{L}(y_i; \theta) = \frac{1}{N} \sum_{i=1}^N \left[\|\mathcal{F}_\Omega G_\theta(y_i) - y_i\|_2^2 + \mathcal{R}(G_\theta(y_i)) \right]. \quad (6)$$

This model can be viewed as an amortization of the instance-specific optimization of Eq. (2), via a neural network G_θ [4,12,19,27,33].

Amortized optimization provides several advantages over classical solutions. First, at test-time, it replaces an expensive iterative optimization procedure with a simple forward pass of a neural network. Second, since the function G_θ is tasked with estimating the reconstruction for any viable input measurement vector y and not just a single instance, amortized optimization has been shown to act as a natural regularizer for the optimization problem [4,33].

3.1 Model Architecture

Similar to instance-based iterative procedures like HQS and supervised unrolled architectures such as [1,32], HQS-Net decouples the minimization of the data consistency term and regularization term in Eq. (6). Specifically, in each iteration block, the network explicitly enforces data consistency preceded by a convolutional block g_{θ_k} that learns an iteration-specific regularization. Thus, we obtain an alternating minimization analogous to Eq. (3):

$$z_k = g_{\theta_k}(x_k), \quad (7a)$$

$$\hat{x}_{k+1}[m] = \begin{cases} \frac{y[m] + \lambda \hat{z}_k[m]}{1 + \lambda}, & \text{if } m \in \Omega \\ \hat{z}_k[m], & \text{else} \end{cases} \quad (7b)$$

where $x_1 = \mathcal{F}_\Omega^H y$ (i.e. the zero-filled reconstruction). Eq. (7b) is implemented as a data-consistency layer (DC) within the network⁶. The unrolled network concatenates $K \in \mathbb{N}$ of these g_{θ_k} and DC blocks, as shown in Fig. 1.

4 Experiments

In our experiments, we used three different MRI datasets: T1-weighted axial brain, T2-weighted axial brain, and PD-weighted coronal knee scans. We applied retrospective down-sampling with 4-fold and 8-fold acceleration sub-sampling masks generated using a Poisson-disk variable-density sampling strategy [9,17,25]. We use 2nd-order and 3rd-order polynomial densities for the 4-fold and 8-fold masks, respectively. All training and testing experiments in this paper were performed on a machine equipped with an Intel Xeon Gold 6126 processor and an NVIDIA Titan Xp GPU.

⁶ For forward models that do not permit an analytical solution of Eq. (7b) (e.g. multi-coil MRI), one can replace the data-consistency layer with an iterative optimization scheme (e.g. conjugate gradient as in [1]). In addition, the iteration-specific weights θ_k in Eq. (7a) can be replaced by a shared set of weights θ , which enforces the model to learn a global regularization prior for all iterations.

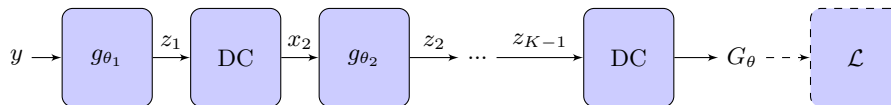


Fig. 1. Proposed architecture. CNN and DC layers are unrolled K times as a deep network, and the final output $G_{\theta} = x_K$ is encouraged to minimize \mathcal{L} defined in Eq. (6). \mathcal{L} does not see fully-sampled data x .

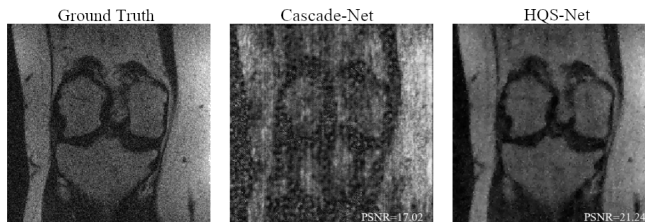


Fig. 2. Example of typical reconstructions of PD-weighted knee for 8-fold acceleration under additive white Gaussian spatial noise, where noise standard deviation $\sigma = 0.1$.

Data. T1-weighted brain scans were obtained from [13], T2-weighted brain scans were obtained from the IXI dataset⁷, and PD-weighted knee scans were obtained from the fastMRI NYU dataset [39]. All images were intensity-normalized to the range $[0, 1]$ and cropped and re-sampled to a pixel grid of size 256×256 . Dataset sizes consisted of 2000, 500, and 1000 slices for training, validation, and testing, respectively.

Comparison Models. We compared the proposed HQS-Net against HQS and Cascade-Net [32], a supervised upper-bound baseline model. All models were implemented in Pytorch.

HQS minimizes the instance-based loss in Eq. (2) using the alternating algorithm in Eq. (3), where the z -minimization is performed using gradient descent. All iterative procedures were run until convergence within a specified tolerance. In choosing $\mathcal{R}(x)$, we followed the literature [25,30] and let

$$\mathcal{R}(x) = \alpha TV(x) + \beta \|Wx\|_1, \quad (8)$$

where TV denotes total variation, W denotes the discrete wavelet transform operator, $\alpha, \beta > 0$ are weighting coefficients, and $\|\cdot\|_1$ denotes the ℓ_1 norm.

Cascade-Net is trained to minimize Eq. (5) using an ℓ_2 loss and with an identical model architecture as HQS-Net. Thus, Cascade-Net requires access to fully-sampled training data, whereas HQS and HQS-Net do not.

For g_{θ_k} , a 5-layer model was used with channel size 64 at each layer. Each layer consists of convolution followed by a ReLU activation function. We used a residual learning strategy which adds the zero-filled input to the output of the

⁷ <https://brain-development.org/ixi-dataset>

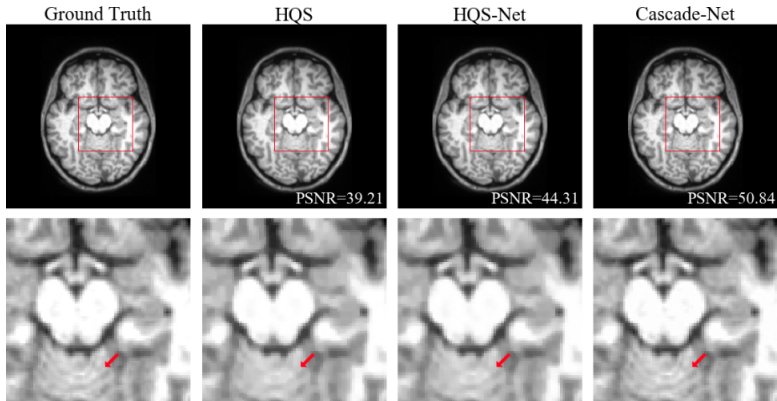


Fig. 3. Example reconstructions of a T1-weighted axial brain slice for 4-fold acceleration. Although classical and unsupervised methods minimize the same loss, the unsupervised model is able to retain more high-frequency detail.

CNN. The overall architecture G_θ is unrolled such that $K = 25$. For training, Adam optimization [22] was used with a learning rate of 0.001 and batch size of 8. In experiments, we set $\lambda = 1.8$, $\alpha = 0.005$, and $\beta = 0.002$, which were optimized using a Bayesian Optimization hyper-parameter tuning package [6].

Evaluation Metrics. Reconstructions were evaluated against ground-truth images on peak signal-to-noise ratio (PSNR), structural similarity index (SSIM) [36], and high-frequency error norm (HFEN) [29]. The *relative* value (e.g., relative PSNR) for a given reconstruction was computed by subtracting the corresponding metric value for the zero-filled reconstruction.

4.1 Results

Runtime and Loss Analysis. Table 1 shows the average runtime and average loss value (defined in Eq. (2) and (8)) achieved by both HQS and HQS-Net on the test set. Since inference for HQS-Net equates to a forward pass through the trained network, HQS-Net is several orders of magnitude faster while achieving superior loss compared to HQS.

Robustness Against Additive Noise. Since HQS-Net does not see fully-sampled data and is trained to minimize a robust classical loss, we expect it to exhibit better performance under circumstances of unseen data and/or noise compared to supervised models. To test this, we artificially inject additive Gaussian noise in both image space and k -space on the test set. Fig. 5 shows a plot of reconstruction quality versus noise variance for 8-fold acceleration. A visual example of the failure of supervised models to perform well under noisy conditions is shown in Fig. 2.

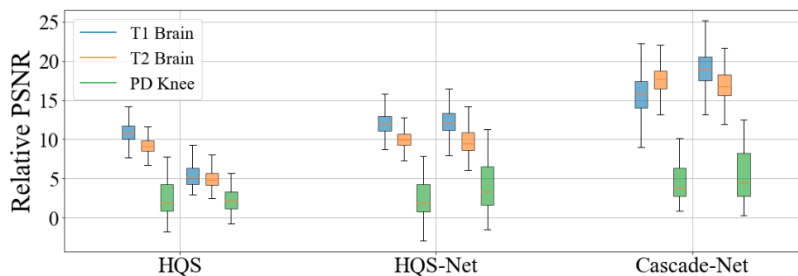
Table 1. Inference runtime and loss. Lower is better. Mean \pm standard deviation across test cases. 4-fold acceleration.

<i>Dataset</i>	<i>Method</i>	<i>Inference time (sec)</i>	<i>Loss</i>
T1 Brain	HQS	483 \pm 111	17.34 \pm 2.94
	HQS-Net	0.241 \pm 0.013	17.20 \pm 2.99
T2 Brain	HQS	380 \pm 72	19.93 \pm 4.20
	HQS-Net	0.246 \pm 0.023	19.46 \pm 4.13
PD Knee	HQS	366 \pm 129	25.28 \pm 10.93
	HQS-Net	0.251 \pm 0.013	24.61 \pm 10.58

Comparison Models. Fig. 4 shows reconstruction performance of all three methods across three datasets. HQS-Net is comparable, if not superior (particularly at high acceleration rates), to the instance-based HQS solver despite the fact that they optimize the same loss function. This may be attributed to the network being trained across many samples, such that it is able to leverage commonalities in structure and detail across the entire training set. Fig. 3 highlights the learning of high-frequency detail.

5 Conclusion

We explored a novel unsupervised MR reconstruction method that performs an amortized optimization of the classical loss formulation for CS-MRI, thus eliminating the need for fully-sampled ground-truth data. We show that our method is more robust to noise as compared to supervised methods that have the same network architecture and is computationally cheaper than classical solvers that minimize the same loss. While our experiments focused on MRI, the method is broadly applicable to other imaging modalities and can be improved with more expressive networks and/or regularization functions.

**Fig. 4.** Reconstruction performance for comparison models of all datasets evaluated on relative PSNR for 4-fold (left) and 8-fold (right) acceleration rates.

Acknowledgements: This research was funded by NIH grants R01LM012719, R01AG053949; and, NSF CAREER 1748377, and NSF NeuroNex Grant1707312.

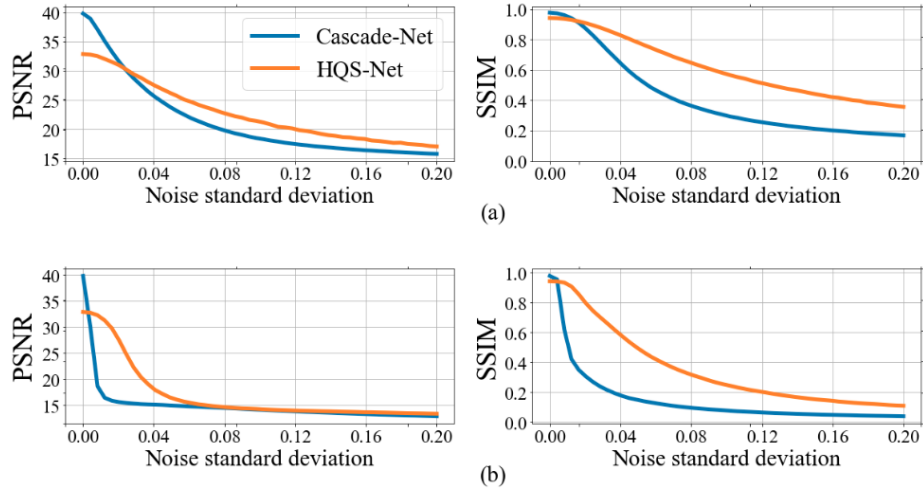


Fig. 5. Average reconstruction performance vs. noise standard deviation for 8-fold acceleration, evaluated on PSNR and SSIM. (a) shows performance under additive noise in image domain and (b) shows performance under additive noise in k -space.

Table 2. Relative Performance. Higher is better. Mean \pm standard deviation across test cases. 4-fold acceleration.

<i>Dataset</i>	<i>Method</i>	<i>PSNR</i>	<i>SSIM</i>	<i>Negative HFEN</i>
T1 Brain	HQS	10.88 \pm 1.256	0.401 \pm 0.052	0.154 \pm 0.016
	HQS-Net	12.10 \pm 1.431	0.409 \pm 0.052	0.157 \pm 0.016
	Cascade-Net	15.72 \pm 2.489	0.416 \pm 0.051	0.180 \pm 0.016
T2 Brain	HQS	9.266 \pm 0.961	0.369 \pm 0.057	0.172 \pm 0.014
	HQS-Net	10.00 \pm 1.055	0.382 \pm 0.057	0.177 \pm 0.015
	Cascade-Net	17.64 \pm 1.910	0.399 \pm 0.056	0.209 \pm 0.017
PD Knee	HQS	2.387 \pm 2.120	0.016 \pm 0.021	0.113 \pm 0.057
	HQS-Net	2.472 \pm 2.117	0.018 \pm 0.021	0.120 \pm 0.054
	Cascade-Net	4.419 \pm 2.081	0.086 \pm 0.023	0.179 \pm 0.048

Table 3. Relative Performance. 8-fold acceleration

<i>Dataset</i>	<i>Method</i>	<i>PSNR</i>	<i>SSIM</i>	<i>Negative HFEN</i>
T1 Brain	HQS	5.403 \pm 1.500	0.161 \pm 0.055	0.303 \pm 0.045
	HQS-Net	12.31 \pm 1.814	0.566 \pm 0.052	0.436 \pm 0.035
	Cascade-Net	15.38 \pm 2.570	0.586 \pm 0.049	0.531 \pm 0.025
T2 Brain	HQS	5.261 \pm 1.520	0.211 \pm 0.050	0.310 \pm 0.055
	HQS-Net	9.880 \pm 1.839	0.553 \pm 0.052	0.457 \pm 0.031
	Cascade-Net	16.92 \pm 1.898	0.589 \pm 0.044	0.576 \pm 0.025
PD Knee	HQS	2.109 \pm 1.277	0.051 \pm 0.040	0.199 \pm 0.094
	HQS-Net	4.019 \pm 2.782	0.085 \pm 0.063	0.252 \pm 0.101
	Cascade-Net	5.393 \pm 3.043	0.156 \pm 0.038	0.347 \pm 0.103

References

1. Aggarwal, H.K., Mani, M.P., Jacob, M.: Modl: Model-based deep learning architecture for inverse problems. *IEEE Transactions on Medical Imaging* **38**(2), 394405 (Feb 2019).
2. Antun, V., Renna, F., Poon, C., Adcock, B., Hansen, A.C.: On instabilities of deep learning in image reconstruction - does ai come at a cost?
3. Bahadir, C.D., Wang, A.Q., Dalca, A.V., Sabuncu, M.R.: Deep-learning-based optimization of the under-sampling pattern in mri. *IEEE Transactions on Computational Imaging* **6**, 1139–1152
4. Balakrishnan, G., Zhao, A., Sabuncu, M.R., Guttag, J., Dalca, A.V.: Voxelmorph: A learning framework for deformable medical image registration. *IEEE Transactions on Medical Imaging* **38**(8), 17881800 (Aug 2019).
5. Beck, A., Teboulle, M.: A fast iterative shrinkage-thresholding algorithm for linear inverse problems. *SIAM J. Img. Sci.* **2**(1), 183202 (Mar 2009).
6. Bergstra, J., Yamins, D., Cox, D.D.: Making a science of model search: Hyperparameter optimization in hundreds of dimensions for vision architectures. In: *Proceedings of the 30th International Conference on International Conference on Machine Learning - Volume 28*. p. I115I123. ICML13, JMLR.org
7. Boyd, S., Parikh, N., Chu, E., Peleato, B., Eckstein, J.: Distributed optimization and statistical learning via the alternating direction method of multipliers. *Found. Trends Mach. Learn.* **3**(1), 1122 (Jan 2011).
8. Chambolle, A., Pock, T.: A first-order primal-dual algorithm for convex problems with applications to imaging. *Journal of Mathematical Imaging and Vision* **40** (05 2011).
9. Chauffert, N., Ciuciu, P., Weiss, P.: Variable density compressed sensing in mri. theoretical vs heuristic sampling strategies. *2013 IEEE 10th International Symposium on Biomedical Imaging* (Apr 2013).
10. Cheng, K., Du, J., Zhou, H., Zhao, D., Qin, H.: Image super-resolution based on half quadratic splitting. *Infrared Physics and Technology* **105**, 103193 (2020).
11. Combettes, P.L., Pesquet, J.C.: Proximal splitting methods in signal processing
12. Cremer, C., Li, X., Duvenaud, D.: Inference suboptimality in variational autoencoders
13. Dalca, A.V., Guttag, J., Sabuncu, M.R.: Anatomical priors in convolutional networks for unsupervised biomedical segmentation. In: *The IEEE Conference on Computer Vision and Pattern Recognition (CVPR)*
14. Daubechies, I., Defrise, M., Mol, C.D.: An iterative thresholding algorithm for linear inverse problems with a sparsity constraint
15. Dong, W., Wang, P., Yin, W., Shi, G., Wu, F., Lu, X.: Denoising prior driven deep neural network for image restoration. *IEEE Transactions on Pattern Analysis and Machine Intelligence* **41**(10), 2305–2318
16. Figueiredo, M.A.T., Nowak, R.D.: An em algorithm for wavelet-based image restoration. *IEEE Transactions on Image Processing* **12**(8), 906–916 (Aug 2003).
17. Geethanath, S., Reddy, R.R.P., Konar, A.S., Imam, S., Sundaresan, R., Ramesh-Babu, R., Venkatesan, R.: Compressed sensing mri: a review. *Critical reviews in biomedical engineering* **41** **3**, 183–204
18. Geman, D., Chengda Yang: Nonlinear image recovery with half-quadratic regularization. *IEEE Transactions on Image Processing* **4**(7), 932–946
19. Gershman, S.J., Goodman, N.D.: Amortized inference in probabilistic reasoning. In: *CogSci*

20. Hammernik, K., Klatzer, T., Kobler, E., Recht, M.P., Sodickson, D.K., Pock, T., Knoll, F.: Learning a variational network for reconstruction of accelerated mri data. *Magnetic Resonance in Medicine* **79**(6), 3055-3071 (Nov 2017).
21. Hu, Y., Jacob, M.: Higher degree total variation (hdtv) regularization for image recovery. *IEEE Transactions on Image Processing* **21**(5), 2559–2571 (May 2012).
22. Kingma, D.P., Ba, J.: Adam: A method for stochastic optimization
23. Lee, D., Yoo, J., Ye, J.C.: Deep residual learning for compressed sensing mri. In: 2017 IEEE 14th International Symposium on Biomedical Imaging (ISBI 2017). pp. 15–18 (April 2017).
24. Liang, D., Cheng, J., Ke, Z., Ying, L.: Deep mri reconstruction: Unrolled optimization algorithms meet neural networks
25. Lustig, M., Donoho, D., Pauly, J.M.: Sparse mri: The application of compressed sensing for rapid mr imaging. *Magnetic Resonance in Medicine* **58**(6), 1182–1195 (2007).
26. Mardani, M., Sun, Q., Vasawanala, S., Pappas, V., Monajemi, H., Pauly, J., Donoho, D.: Neural proximal gradient descent for compressive imaging
27. Marino, J., Yue, Y., Mandt, S.: Iterative amortized inference
28. Nikolova, M., Ng, M.K.: Analysis of half-quadratic minimization methods for signal and image recovery. *SIAM Journal on Scientific Computing* **27**(3), 937–966 (2005).
29. Ravishanker, S., Bresler, Y.: Mr image reconstruction from highly undersampled k-space data by dictionary learning. *IEEE Transactions on Medical Imaging* **30**(5), 1028–1041 (May 2011).
30. Ravishanker, S., Ye, J.C., Fessler, J.A.: Image reconstruction: From sparsity to data-adaptive methods and machine learning. *Proceedings of the IEEE* **108**(1), 86109 (Jan 2020).
31. Rudin, L.I., Osher, S., Fatemi, E.: Nonlinear total variation based noise removal algorithms. *Physica D Nonlinear Phenomena* **60**(1-4), 259–268 (Nov 1992).
32. Schlemper, J., Caballero, J., Hajnal, J.V., Price, A., Rueckert, D.: A deep cascade of convolutional neural networks for mr image reconstruction. *Information Processing in Medical Imaging* p. 647658 (2017).
33. Shu, R., Bui, H.H., Zhao, S., Kochenderfer, M.J., Ermon, S.: Amortized inference regularization
34. Tezcan, K.C., Baumgartner, C.F., Luechinger, R., Pruessmann, K.P., Konukoglu, E.: Mr image reconstruction using deep density priors. *IEEE Transactions on Medical Imaging* **38**(7), 16331642 (Jul 2019).
35. Wang, S., Su, Z., Ying, L., Peng, X., Zhu, S., Liang, F., Feng, D., Liang, D.: Accelerating magnetic resonance imaging via deep learning. In: 2016 IEEE 13th International Symposium on Biomedical Imaging (ISBI). pp. 514–517 (April 2016).
36. Wang, Z., Bovik, A.C., Sheikh, H.R., Simoncelli, E.P.: Image quality assessment: From error visibility to structural similarity. *Trans. Img. Proc.* **13**(4), 600612 (Apr 2004).
37. Yang, Y., Sun, J., Li, H., Xu, Z.: Admm-net: A deep learning approach for compressive sensing mri
38. Ye, N., Roosta-Khorasani, F., Cui, T.: Optimization methods for inverse problems. *MATRIX Book Series* p. 121140 (2019).
39. Zbontar, J., Knoll, F., Sriram, A., Murrell, T., Huang, Z., Muckley, M.J., Defazio, A., Stern, R., Johnson, P., Bruno, M., Parente, M., Geras, K.J., Katsnelson, J., Chandarana, H., Zhang, Z., Drozdal, M., Romero, A., Rabbat, M., Vincent, P., Yakubova, N., Pinkerton, J., Wang, D., Owens, E., Zitnick, C.L., Recht, M.P., Sodickson, D.K., Lui, Y.W.: fastmri: An open dataset and benchmarks for accelerated mri